

OPEN

Effects of Structural Factors of Hydrated TiO₂ on Rutile TiO₂ Pigment Preparation via Short Sulfate Process

Congxue Tian^{1,2}

The structural factors such as crystal structure, particle size distribution and impurity content of hydrated TiO₂ had great effects on the structures and pigment properties of the rutile TiO₂. The rutile TiO₂ white pigment was prepared via the Short Sulfate Process from low concentration industrial TiOSO₄ solution. In order to produce rutile TiO₂ pigment with good structures and excellent pigment properties, the crystal size of the hydrated TiO₂ should be controlled less than 8.9 nm and as close as possible to 7.9 nm, which could effectively promote the phase transformation and crystal growth of the rutile TiO₂. The appropriate particle size distribution of hydrated TiO₂ had obvious effects on obtaining rutile TiO₂ with narrower particle size distribution and near 0.20 μm. It was best to adjust the hydrolysis conditions to reduce the specific surface area of the hydrated TiO₂ so as to reduce the iron ion impurity adsorption.

In the material science, the material's properties are determined by their structural factors, such as the crystal structure, phase composition, chemical composition, and so on, its essence is the reflection of material structure theory. And the structural factors would be determined by the preparation process and controlling conditions, which would ultimately determine the properties and applications of the materials. Titanium dioxide (TiO₂) is the third largest commercial inorganic chemicals, either in anatase or rutile polymorphs, and due to its excellent properties such as higher refractive index, smaller crystal size, better optical properties and chemical inertness, it has become the most widely used white pigments, used in many fields such as coatings, paints, paper, fibers, cosmetics, sunscreen products, chemical catalysis, electronic materials and so forth¹⁻³. Titanium dioxide white pigment is commercially prepared by either chloride process or sulfate process. In recent year, the market demand of titanium dioxide increases by about 3% every year. In 2019, the global titanium dioxide production capacity was 8,685,000 tons, the production capacity was of 3,845,000 tons and the output was of 3,137,200 tons in China in 2019, and the output of the sulfate process accounting for 93.6% in China. The core step for titanium dioxide production via the sulfate process is the hydrolysis of the titanyl sulfate solution. The hydrolysis process would undergo a series of complex physical and chemical reactions, and the hydrolysis parameters and conditions would have great effects on the structure of the hydrolysis products (hydrated TiO₂, also named metatitanic acid), and the structure and quality of hydrated TiO₂ would ultimately determine the structure and properties of the titanium dioxide pigment. And the thermal hydrolysis reactions of industrial TiOSO₄ solution include nucleation, crystal growing, polymerization, agglomeration, aggregation and precipitation, accompanied by hydrolysis precipitation of crystalline TiO²⁺ ions via ololation and oxolation reaction⁴. Researches show that the hydrated TiO₂ is colloidal particles, formed by nuclei growing and aggregating, and eventually forming the secondary aggregated particles with the particle size of 10–200 μm^{5,6}. Many researchers have widely investigated the hydrolysis process and conditions, effects of the additives and hydrolysis parameters on the products, as well as properties and applications of titanium dioxide⁷⁻¹⁶. Urakaev *et al.* investigated the homogeneous nucleation and growth of monodispersed spherulites of sulphur and hydrated titanium dioxide of anatase modification by a new coherent optical method for measurement of the relative scattering coefficient based on alternative use of laser radiation of various wavelengths¹⁷. Ultrasonic technology was used to pretreat hydrated TiO₂ slurry before washing, which showed that the removal effect of iron impurities in hydrated TiO₂ was better and the effect of washing water

¹Panzhuhua University, Panzhuhua, 617000, Sichuan, China. ²Key Laboratory of Green Chemistry of Sichuan Institutes of Higher Education, Zigong, 643000, Sichuan, China. e-mail: tcx7311@163.com

saving was obvious, while the lattice parameters of TiO_2 had no effect on rutile and product quality¹⁸. The effects of ball milling process parameters and stress energy on the particle size distribution of TiO_2 were investigated, and the results showed that particle size distribution had greatly influenced the pigment performances¹⁹. The particle size and its distribution of TiO_2 had prominently affected its spectral reflectance and color coordinates, and a model was established to investigate the effect of particle size on the aesthetic and thermal properties of poly-dispersed titanium dioxide pigments coatings²⁰. By investigating the precipitation and growth behavior of hydrated TiO_2 hydrolyzed from titanyl sulfate solution, the hydrolysis temperature was the most important factor affecting the particle size of hydrated TiO_2 , and the hydrated TiO_2 particles were easy to aggregate in the preparation process, which could be described by an empirical expression²¹. The physicochemical properties of anatase TiO_2 nanoparticles could also be changed by using surface treatment²². However, there were few reports about the effects of the structural factors of hydrated TiO_2 on the pigment properties. The short sulfate process refers to the titanium dioxide preparation by using unenriched low concentration TiOSO_4 solution as titanium source via sulfate process, cancelling the concentration section of diluted TiOSO_4 solution, having the advantages of short process, low cost and low energy consumption, which could promote the technological innovation of traditional sulfate process for TiO_2 pigment production^{23,24}.

The structures of the hydrated titanium dioxide had great impacts on TiO_2 production. Herein, hydrated TiO_2 was prepared via short Sulfate Process by using the unenriched low concentration TiOSO_4 solution as raw material to produce rutile TiO_2 pigment. It was important to investigate the influences of the crystal structure, particle size distribution and impurity of the hydrated TiO_2 on the TiO_2 pigment preparation.

Experimental

Rutile TiO_2 pigments were prepared from different low concentration industrial TiOSO_4 solution (the total TiO_2 concentration ranging from 155 g/L to 180 g/L, weight concentration) as titanium sources, through thermal hydrolysis by authigenic seed method via the Short Sulfate Process. The typical hydrolysis process was carried out as listed in our literature²³, and the pre-adding water volume ratio (as water to TiOSO_4 solution) was of 0.18:1, the hydrolysis time after the second boiling point was of 2.5 h, then finished the hydrolysis process and obtained the hydrated TiO_2 . The as-prepared hydrated TiO_2 was washed with water, bleached and filtered, then whipped to slurry with the deionized water uniformly. The slurry was doped with the rutile calcining seed (5%, as to TiO_2 , wt %), zinc salt (ZnO of 0.26%), potassium salt (K_2O of 0.50%) and phosphate salt (P_2O_5 of 0.11%), then calcined in a muffle furnace in the air atmosphere. The calcining conditions was as the following: firstly from room temperature raising to 420 °C in 60 min and holding for 30 min at 420 °C, secondly from 420 °C to 780 °C in 60 min and holding for 60 min at 780 °C, and lastly from 780 °C to 870 °C in 120 min and holding for 40 min. Then the rutile TiO_2 pigment powder was obtained after cooling and grinding by the three head grinder. The different concentration of industrial TiOSO_4 solution was conducted at 155 g/L, 161 g/L, 167 g/L, 173 g/L, 180 g/L, and the obtained hydrated TiO_2 samples were marked as A, B, C, D, E, the rutile TiO_2 samples after salt treatment and calcination were denoted as A1, B1, C1, D1, E1, respectively.

The crystal structures of hydrated titanium dioxide and rutile TiO_2 were determined by the XRD analysis (X'Pert3 Powder, PANalytical), and the crystal size $L_{(101)}$ for the anatase crystal plane (101) of hydrated TiO_2 and $L_{(110)}$ for rutile TiO_2 crystal plane (110) was calculated according to Scherrer equation (Eq. A), where K was the constant (0.8900), λ was the wavelength of $\text{CuK}\alpha_1$ (0.15418 nm), β was the full width at half maximum intensity (FWHM) of crystal plane for XRD peak in radians, and θ was the Bragg's diffraction angle, respectively. The rutile content (X_R) was calculated according to Eq. B, where I_A and I_R represented the integrated intensity of the anatase (101) main peak and the rutile (110) main peak, respectively.

$$\text{Crystal size: } L = K\lambda/\beta \cdot \cos\theta \quad (\text{A})$$

$$\text{Rutile phase content: } X_R = I_R/0.884I_A + I_R \quad (\text{B})$$

Particle size distribution (PSD) test was carried out on a Malvern particle size analyzer (Malvern Zetasizer Nano ZS90). The specific surface area of hydrated TiO_2 was measured on the surface and pore size distribution instrument (3H-2000PS1, Beishide, China). The S_{BET} of the hydrated TiO_2 samples were calculated by the BET multi-point method according to the N_2 adsorption-desorption curves. The UV-vis diffuse reflection spectra were obtained on a ultraviolet visible spectrophotometer with integral ball accessories (U-4100, Hitachi). The particle morphology was observed on a JEOL scanning electron microscopy (JSM-7100F). The surface morphology was carried out on a field emission transmission electron microscopy (Tecnai G2 F20S-TWIN) at 200 kV. The impurities of the rutile samples was determined on an ICP-AES (ICAP 6300, Thermo Scientific Co. Ltd). The ultra-precise colorimeter (LabScan EX, American Hunter) was used to determine the pigment properties, such as the chromatic power (TCS), blue phase (SCX), the brightness ($Jasn$) and the relative scattering force (R_s), by using the R930 (Ishihara Sangyo Kaisha, Ltd.) as the standard reference sample.

Results and Discussions

Crystal structure. The crystal structure of the obtained hydrated TiO_2 had great impacts on the crystal structure of titanium dioxide pigment, and would ultimately affect the pigment properties of titanium dioxide. The XRD patterns of the as-prepared hydrated TiO_2 series were showed in Fig. 1, and the XRD patterns for rutile TiO_2 in Fig. 2. The crystal size for anatase $L_{(101)}$ of hydrated TiO_2 , and the crystal size for rutile $L_{(110)}$, the rutile content X_R and pigment properties for rutile TiO_2 white pigment were listed in Table 1.

In the hydrolysis system to produce titanium dioxide pigment, the hydrolysis intermediates (also named hydrated TiO_2 , or metatitanic acid) would absorb a large amount of water and sulfate anion to form the crystalline structure with anatase phase, due to the presence of a large number of sulfate anion in the hydrolysis system, with

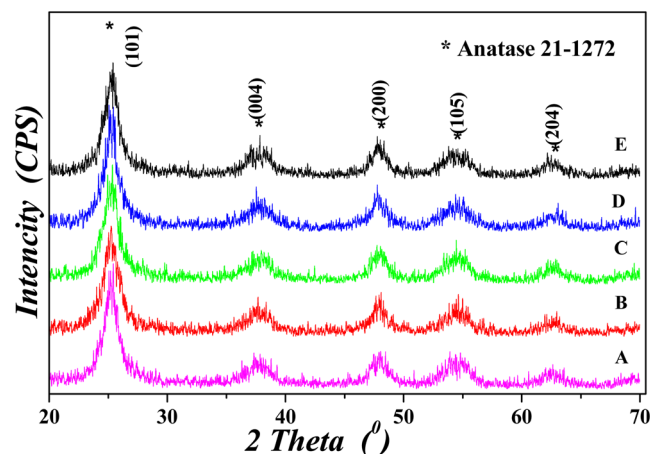


Figure 1. XRD patterns for the hydrated TiO_2 .

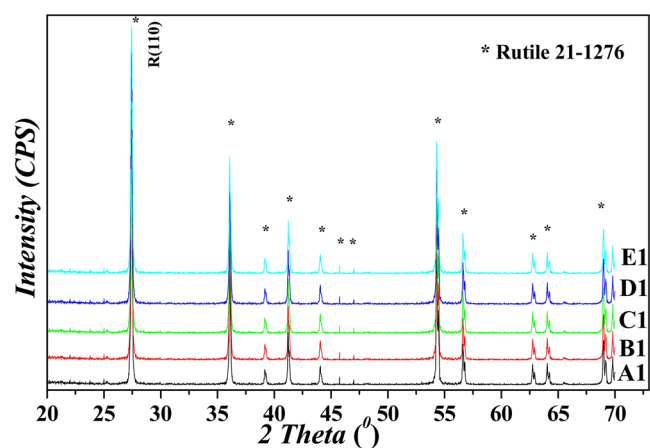


Figure 2. XRD patterns for the rutile TiO_2 pigments.

Hydrated TiO_2	$L_{(101)}$ (nm)	Rutile TiO_2	X_R (%)	$L_{(110)}$ (nm)	TCS	SCX	Jasn
A	8.42	A1	98.5	124.2	1780	2.25	94.54
B	8.14	B1	98.8	134.1	1820	2.56	94.86
C	7.83	C1	99.1	142.4	1840	3.18	95.17
D	7.57	D1	99.4	147.6	1810	2.64	94.93
E	7.10	E1	99.9	158.3	1700	2.19	94.68
R930	/	R930	/	/	1910	3.12	94.52

Table 1. Crystal size, rutile content and pigment properties for hydrated TiO_2 and rutile TiO_2 pigment.

the molecular structure as $\text{H}_2\text{TiO}_3 \cdot \text{H}_2\text{O}$. In Fig. 1, all the XRD patterns of the hydrated TiO_2 samples were clearly consistent with the standard anatase TiO_2 phase (JCPDS 21–1272), without any other crystal phase diffraction peaks, showing with only the anatase phase. The hydrated TiO_2 was anatase phase with low crystallinity due to their wide flat diffraction peaks and low diffraction intensity. The crystal size $L_{(101)}$ for hydrated titanium dioxide ranged from 8.42 nm to 7.10 nm. Hydrated titanium dioxide was transformed into rutile TiO_2 structure after salt treatment and calcinations, and the rutile crystal phase structure was consistent with the standard rutile TiO_2 (JCPDS 21–1276). Due to the difference of crystal size, particle size distribution and impurity content for metatitanic acid, there was a small deviation in the rutile crystallization process during the calcination process, resulting in a small deviation in the XRD pattern. The rutile content (X_R) increased gradually with the decreasing of the crystal size $L_{(101)}$ of hydrated titanium dioxide (as listed in Table 1). The negative linear correlation between X_R and $L_{(101)}$ were shown in Eq. (1). In the equation, R represented as the correlation coefficient and SD represented as the standard deviation.

$$X_R = 107.42 - 1.06 * L_{(101)}, R = 0.9998, SD = 0.01362 \quad (1)$$

When the crystal size of hydrated TiO₂ was small, it was easier to transform into rutile TiO₂ crystalline by surface atom diffusion during calcination process due to its higher crystal surface energy. In the calcination process, the phase transformation from anatase to rutile was mainly through the surface atomic diffusion, in order to use the atomic reconstruction to reduce the energy of the crystal and form a stable rutile structure. When rutile crystal nucleus was formed, the TiO₂ crystal ions continuously aggregated and grew on the newly formed rutile crystal nucleus through surface atom diffusion, which would make the rutile titanium dioxide crystal growing. And at the same conditions, the smaller crystal size of hydrated TiO₂ needed the lower calcination conditions and strength for crystal phase transformation from anatase to rutile. In order to meet the requirement of rutile content for rutile TiO₂ production ($X_R > 98\%$), the anatase crystal size of the hydrolyzed hydrated TiO₂ should be controlled below 8.89 nm. However, when the crystal size of hydrated TiO₂ was too small and with obvious colloidal properties, the calcined particles would be easily sintering to form larger rutile titanium dioxide particles, resulting in deteriorating the rutile TiO₂ pigments properties.

The negative linear mathematical relationship of crystal size between $L_{(110)}$ for the rutile TiO₂ and $L_{(101)}$ for the hydrated TiO₂ was as the following, Eq. (2).

$$L_{(110)} = 338.79 - 25.28 * L_{(101)}, R = 0.9943, SD = 1.595 \quad (2)$$

From Eq. (2), as crystal size decreasing of hydrated TiO₂, it would be easy to transform hydrated TiO₂ to rutile structure and promote the atomic diffusion in the calcination process basing on the high surface energy of hydrated TiO₂, which would make the phase transformation and crystal growth of rutile TiO₂ easier and obtain the larger rutile crystals. On the other hand, it would be easier to cause the sample sintering and agglomerate to form larger particles when the crystal size of hydrated TiO₂ was too small.

The pigment properties of rutile TiO₂ pigments (also named initial product) were mainly determined by its crystal structure, particle size and its distribution. The chromatic power (*TCS*) of the calcined rutile TiO₂ products ranged from 1700 to 1840. Without coating post-treatment, the *TCS* values for the rutile samples were lower than the reference sample R930 which was with coating post-treatment. The *TCS* of the samples increased firstly and then decreased as the crystal size of hydrated TiO₂ decreasing gradually. The mathematical relationship between *TCS* and $L_{(101)}$ was as the following equation, Eq. (3).

$$TCS = -11415.26 + 3354.25 * L_{(101)} - 212.26 * L_{(101)}^2, R^2 = 0.9959, SD = 4.983 \quad (3)$$

Equation (3) showed quadratic linear relationship with high fitting degree. After taking the derivation, it showed that the maximum value of *TCS* was of 1836.2 (about 1840) when the crystal size of hydrated TiO₂ was of 7.90 nm, indicating that the pigment properties of rutile TiO₂ were partly determined by the structure of hydrated TiO₂. And the crystal size of hydrated TiO₂ could be controlled in an appropriate range by adjusting the hydrolysis conditions such as the number and quality of the hydrolysis seeds, concentration of TiOSO₄ solution and hydrolysis time, which could effectively improve the product pigment properties. It could also approximately predict the pigment properties according to crystal size of hydrated TiO₂ under certain conditions.

The blue phase (*SCX*) of the rutile pigment showed a similar changing trend as that of *TCS*, which was gradually increasing from 2.25 to 3.18, and then decreasing to 2.19. It was harmful for phase transformation from anatase to rutile and rutile crystal growth during calcination process when the crystal size of hydrated TiO₂ was too large or too small. Because of the inconsistent phase transformation and growth of rutile crystal, it was easier to cause uneven growth of rutile TiO₂ crystalline grain, ultimately reducing its sintering resistance and the *SCX* value. The brightness index (*Jasn*) of the calcined products was better and higher than that of the reference sample R930 (94.52). The *Jasn* also showed the same changing trend as that of *TCS*, increasing gradually to 95.17 at first and then decreasing to 94.68.

Appropriate crystal structure and suitable crystal size of hydrated TiO₂ were helpful to promote the phase transformation from anatase to rutile and the rutile crystal growth during the calcination process to obtain good rutile TiO₂ crystalline structure, resulting in proper crystal size of the rutile titanium dioxide. The integrity of rutile crystal structure ensured its high refractive index and scarcely any sintering particles, which could improve the calcination process and obtain rutile TiO₂ with suitable particle size distribution and better crystal structure. All these influencing factors were helpful to improve the rutile pigment properties.

Particle size distribution and impurity iron content. The particle size distribution (*PSD*) of the rutile titanium dioxide also had important influences on the pigment properties. Because the *TCS* of the rutile TiO₂ was related to the light scattering coefficient (*S*) and the light absorption coefficient (*K*), the larger of *S* value and the smaller of *K* value, the larger of *TCS*, and the better of the covering power and whiteness of the titanium dioxide pigment²⁵. Generally, in order to improve the *S* value, the particle size of the pigment should be controlled in the range of 0.15–0.35 μm in the visible light range, and the amount and content of titanium dioxide particles should be maintained as higher as possible in the range about 0.2 μm. The average particle size (D_{AV}), particle polydispersity (*Pdi*), relative scattering force (R_s) and impurities content of the calcined rutile TiO₂ pigments were showed in Table 2.

The D_{AV} of hydrated TiO₂ ranged from 0.782 μm to 1.130 μm. The polydispersity (*Pdi*) was used to characterize the particle size distribution of the mono-dispersity particles, and the smaller the value was, the more concentrated particle size distribution was. The *Pdi* value was the index indicating the wide and narrow of particle size distribution, the smaller the *Pdi* value was, the narrower the *PSD* was. The *Pdi* of hydrated TiO₂ ranged from 0.132 to 0.475, and sample C was the smallest with the narrowest *PSD*. The D_{AV} of the calcined rutile TiO₂ ranged from

Hydrated TiO ₂	D _{AV} nm	Pdi	S _{BET} m ² /g	Fe %	Rutile TiO ₂	D _{AV} nm	Pdi	Wt,% (0.15–0.30 μm)	Fe %	ZnO %	K ₂ O + Na ₂ O %	P ₂ O ₅ %	R _s %
A	1130	0.433	275	0.0042	A1	339	0.362	66.8	0.0040	0.2295	0.1522	0.1025	97.8
B	976	0.341	256	0.0022	B1	307	0.265	71.4	0.0021	0.2283	0.1519	0.1021	98.4
C	782	0.132	243	0.0012	C1	238	0.107	78.2	0.0011	0.2272	0.1526	0.1018	99.2
D	887	0.369	267	0.0034	D1	321	0.303	69.7	0.0033	0.2279	0.1531	0.1020	97.9
E	1029	0.475	282	0.0052	E1	372	0.387	64.1	0.0050	0.2284	0.1534	0.1022	97.1
R930	/	/	/	/	R930	/	/	/	/	/	/	/	100

Table 2. Effect of particle size distribution and impurities content of hydrated TiO₂ on rutile TiO₂ pigment.

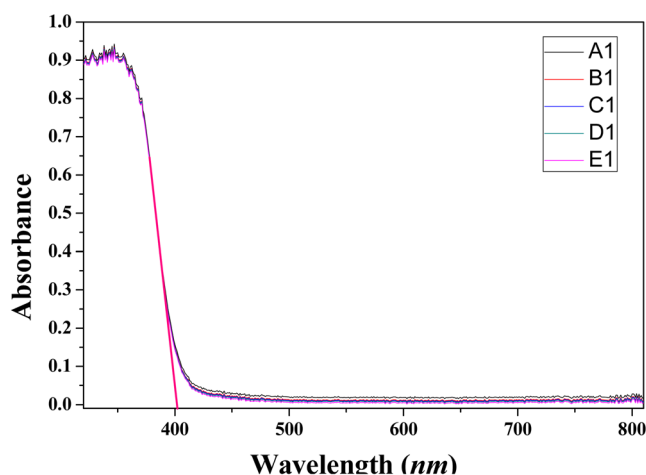


Figure 3. UV-vis diffuse reflection spectra for the rutile TiO₂ pigments.

0.238 μm to 0.372 μm, with the *Pdi* value ranging from 0.107 to 0.387, of which sample C1 had the narrowest *PSD* with *Pdi* of 0.107. It showed that the *Pdi* value of titanium dioxide prepared by hydrated TiO₂ with smaller *Pdi* value was also smaller than the others (Table 2), which indicated that narrower *PSD* of hydrated TiO₂ was beneficial to obtain TiO₂ powders with narrower *PSD*. The *Pdi* values for hydrated TiO₂ and rutile TiO₂ were met with the following mathematical relationships.

$$Pdi_{TiO_2} = -0.00554 + 0.82955 * Pdi_{MA}, R = 0.9975, SD = 0.00893 \quad (4)$$

The relationships of *Pdi* showed positive linear correlation (Eq. (4)). Narrower *PSD* of hydrated TiO₂ was beneficial to control the crystal phase transformation and crystal growth of rutile TiO₂ in a suitable uniform range during the calcination process. When the *PSD* of hydrated TiO₂ was narrower, as the particle size was more uniform in the calcining process, and the properties and compositions of the active sites of anatase TiO₂ in the phase transformation and crystal growth were closer, by atomic diffusion and crystal growth on the particle's surface, the obtained calcined rutile particles were uniform. Ultimately, the obtained calcined rutile TiO₂ was with narrower and more uniform *PSD*, which could effectively improve the pigment properties. While when the *PSD* of hydrated TiO₂ became wider, the *PSD* of the calcined rutile TiO₂ became wider due to the inconsistent diffusion process and crystal growth during the calcining process, which ultimately deteriorated the pigment properties. The mass content of titanium dioxide with particle size distribution in the range of 0.15–0.30 μm was listed in Table 2. This further proved that when the *PSD* was narrower, the higher the mass ratio of particles in the suitable size range for rutile TiO₂ products, the better the corresponding pigment properties. The relative scattering force (*R_s*) refers to the ratio of the scattering ability of a pigment to the incident light in a certain medium compared with the reference pigment, and the larger the ratio, the better the pigment performance. The relationship between *R_s* and *D_{AV,TiO2}* was as the following equation.

$$R_s = 102.96 - 0.01547 * D_{AV,TiO_2}, R = 0.9857, SD = 0.1516 \quad (5)$$

The relationship between *R_s* and *D_{AV,TiO2}* showed negative linear correlation (Eq. (5)). In order to improve the *R_s* value, it was necessary to control the product particle size near 0.20 μm calculated from Eq. (5) and maintain it in a narrow *PSD* range, so as to obtain rutile TiO₂ with excellent pigment properties.

The UV-vis spectra for the rutile TiO₂ pigments were showed in Fig. 3. The absorption spectra for all the samples were consistent, there was a strong absorption in the wavelength region less than 402.4 nm, and the difference of absorption intensity was not significant. This part of absorption corresponded to the intrinsic absorption of rutile titanium dioxide, which was the energy absorbed by the electron transition from the valence band of

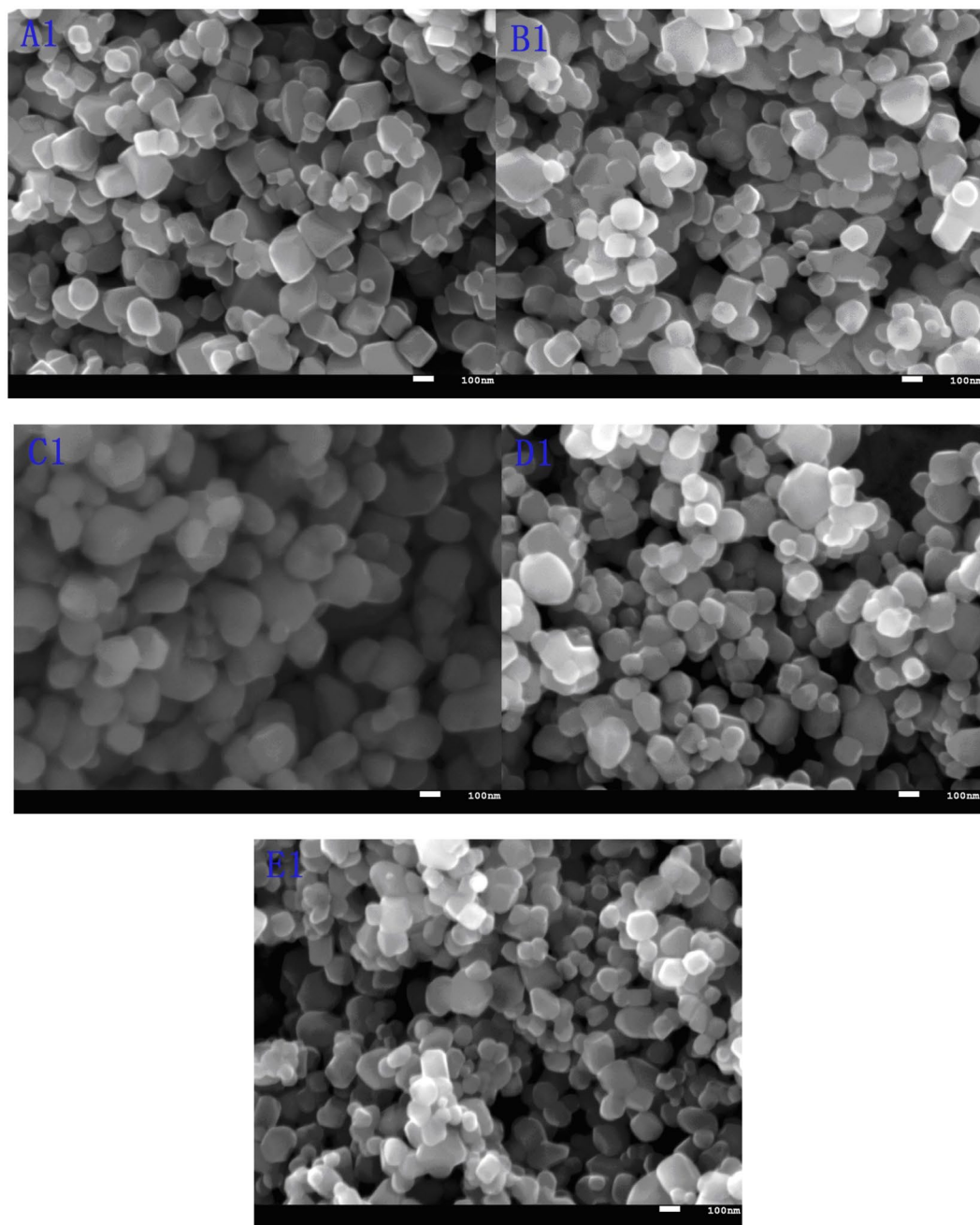


Figure 4. SEM photographs for rutile TiO₂ pigment.

titanium dioxide to the conduction band (the intrinsic forbidden band width, 3.08 eV). The fine fluctuation of the absorption spectra might be caused by different sizes of the rutile crystals.

The SEM photographs for the rutile samples were shown in Fig. 4. All the particles showed rutile TiO₂ morphologies with clearly crystal contour, and the high crystalline was consistent with the XRD analysis. The particle size ranges from 70 nm to 300 nm, and the main average particle size was of about 120 nm. During the calcination process, the smaller particles might congregate together to form a larger one due to re-crystallization because its higher surface energy and crystal growth drive, resulting in larger particle size and larger D_{AV} , as showing in Table 2. It could be seen that the larger and wider the particle size of hydrated TiO₂ was, the wider PSD of rutile TiO₂ products was, resulting in poor pigment properties, as listed in Tables 1 and 2. And sample C1 was with the narrowest PSD and the smallest Pdi , and it confirmed that the appropriate PSD for the hydrated TiO₂ would improve the crystal growth and PSD for rutile TiO₂. This also proved that appropriate particle size and narrow PSD of hydrated TiO₂ were conducive to obtaining narrower and uniform particle size distribution of rutile TiO₂, and reducing sintering phenomena for the particles, which would lead to improve the pigment properties. The regular crystallographic perfection, good and complete morphology, proper PSD for TiO₂ was all beneficial to improve pigment properties.

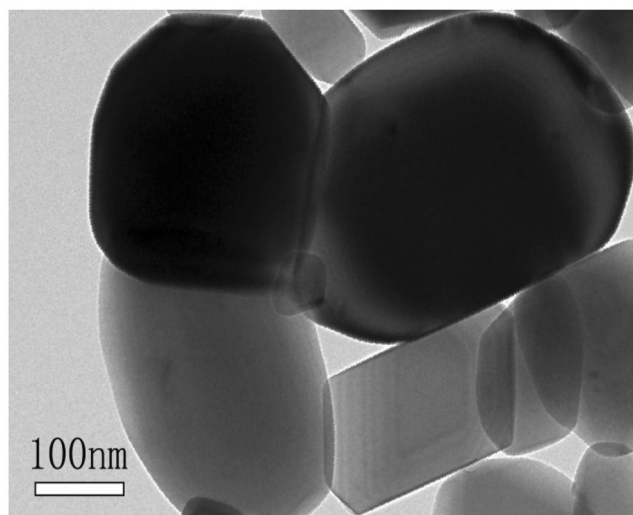


Figure 5. TEM photograph for sample C1.

The TEM photograph for sample C1 was showed in Fig. 5. The crystal profile of sample C1 was clear, and the particle uniformity was good. The average size was about 240 nm, which was consistent with the particle size test results. The size of particles was different, which might be related to the slow hydrolysis rate and uneven hydrolysis process of TiOSO_4 solution. Better particle morphology and particle size distribution would contribute to the improvement of the pigment performances.

Because the hydrolyzed hydrated TiO_2 was with small size of crystal and aggregates, large specific surface area and stronger colloidal properties, the impurities were easy to be adsorbed on and brought out by hydrated TiO_2 . As the adsorbed amount of colored impurities was one of the key factors affecting the structure of titanium dioxide, it was of great importance to improve pigment properties by controlling the adsorbed impurities in an appropriate range. The iron impurity was the main colored impurity, and when the content exceeded the limited range (commonly less than 30 ppm for rutile TiO_2 and less than 90 ppm for anatase TiO_2), it would cause the rutile samples yellowing and sintering, which would seriously worsen the pigment performances. The main impurities content including Fe, ZnO, $\text{K}_2\text{O} + \text{Na}_2\text{O}$ and P_2O_5 of the rutile TiO_2 pigments were listed in Table 2, and the content of these impurities was low, which had little effect on the properties of the rutile TiO_2 pigments. The specific surface area (S_{BET}) was a key factor that affecting the adsorbed amount of impurities. The adsorbed content of iron ions gradually increased with the increasing of the S_{BET} for hydrated TiO_2 (as showed in Table 2). The relationship between the adsorption amount of impurity iron (% Fe) and the S_{BET} of hydrated titanium dioxide was as the following equation.

$$\%Fe = -0.02371 + 1.01839 * 10^{-4} * S_{\text{BET}}, R = 0.9948, SD = 0.0001869 \quad (6)$$

The % Fe had positive linear correlation with the S_{BET} of hydrated TiO_2 . The S_{BET} of the hydrated TiO_2 should be as small as possible in order to control the % Fe. The S_{BET} of hydrated TiO_2 was connected with the hydrolysis conditions and operational parameters. When the hydrolysis conditions were well controlled, the hydrolysis reaction was conducted more uniform, the precipitated hydrated TiO_2 particles were more well-distributed and the formed aggregates were with narrower particle size distribution and relative smaller S_{BET} . At the same time, the colloidal properties of hydrated TiO_2 would be weakened by increasing the hydrolysis temperature and prolonging the hydrolysis time, which could reduce the S_{BET} and adsorption amount of impurity iron, resulting in better pigment properties. In addition, it was also great important that hydrated TiO_2 with narrower particle size distribution and smaller S_{BET} , which could be conducive to reduce the subsequent washing water consumption, shorten the washing time and reduce the washing strength and cost.

Conclusions

The rutile TiO_2 pigments were prepared through thermal hydrolysis by authigenic seed method via Short Sulfate Process. The structural factors such as crystal structure, particle size distribution, impurity content of the iron ion and specific surface area of the hydrated titanium dioxide had great important impacts on the crystal structure, pigment properties and PSD of the rutile TiO_2 , and there had also an internal influencing relationship among these factors, these factors influenced and determined each other. Suitable crystal size and crystal structure of the hydrolyzed hydrated TiO_2 were helpful to promote the phase transformation from anatase to rutile and crystal growth of rutile TiO_2 , and it was also related to the rutile content, crystal size and pigment properties of rutile TiO_2 satisfying with mathematical regression correlation. It was advisable to control the crystal size of hydrated to be less than 8.9 nm and close to 7.9 nm, which could obtain rutile TiO_2 with good crystal structure which could reduce the sintering of the particles and enhance the pigment performances for rutile TiO_2 pigments. The appropriate particle size and particle size distribution of hydrated TiO_2 had obvious effects on the particle size distribution, polydispersity and relative scattering force of the rutile TiO_2 particles. The adsorption amount of

impurity iron ions was greatly affected by the S_{BET} of hydrated TiO_2 , and there was a correlation relationship between them. Rutile titanium dioxide pigments with good structure, regular morphology and excellent pigment properties could be prepared by controlling the hydrolysis conditions to obtain hydrated TiO_2 with the particle size distribution as much narrower as possible, and lower impurity content of iron. Appropriate structural factors of hydrated TiO_2 were helpful to prepare titanium dioxide with excellent pigment properties.

Received: 16 February 2020; Accepted: 15 April 2020;

Published online: 14 May 2020

References

- Buxbaum, G. & Pfaff, G. Industrial Inorganic Pigments, Third, Completely Revised Edition, Chapter 2.1 Titanium Dioxide, 51–81 (WILEY-VCH Verlag GmbH & Co. KGaA, Weinheim 2005).
- Jalava, J. P. The use of an exact light-scattering theory for spheroidal TiO_2 pigment particles. *Particle & Particle Systems Characterization* **23**, 159–164, <https://doi.org/10.1002/ppsc.200601025> (2006).
- Wang, Y., Li, J., Wang, L., Xue, T. & Qi, T. Preparation of rutile titanium dioxide white pigment via doping and calcination of metatitanic acid obtained by the NaOH molten salt method. *Industrial & Engineering Chemistry Research* **49**, 7693–7696, <https://doi.org/10.1021/ie1007147> (2010).
- Santacesatia, E., Tonello, M., Storti, G., Pace, R. C. & Carra, S. Kinetics of titanium dioxide precipitation by thermal hydrolysis. *Journal of Colloid and Interface Science* **111**, 44–53, [https://doi.org/10.1016/0021-9797\(86\)90005-6](https://doi.org/10.1016/0021-9797(86)90005-6) (1986).
- Sathyamoorthy, S., Hounslob, M. J. & Moggridge, G. D. Influence of stirrer speed on the precipitation of anatase particles from titanyl sulphate solution. *Journal of Crystal Growth* **223**, 225–234, [https://doi.org/10.1016/S0022-0248\(01\)00619-4](https://doi.org/10.1016/S0022-0248(01)00619-4) (2001).
- Przepiera, A., Jablonski, M. & Wisniewski, M. Study of kinetics of reaction of titanium raw-materials with sulfuric-acid. *Journal of Thermal Analysis And Calorimetry* **40**, 1341–1345, <https://doi.org/10.1007/BF02546898> (1993).
- Tian, C. X. Internal influences of hydrolysis conditions on rutile TiO_2 pigment production via short sulfate process. *Materials Research Bulletin* **103**, 83–88, <https://doi.org/10.1016/j.materresbull.2018.03.025> (2018).
- Garg, A. et al. Photocatalytic degradation of bisphenol-A using N, Co codoped TiO_2 catalyst under solar light. *Scientific Reports* **9**, 765, <https://doi.org/10.1038/s41598-018-38358-w> (2019).
- Kim, E. J. et al. Thorn-like TiO_2 nanoarrays with broad spectrum antimicrobial activity through physical puncture and photocatalytic action. *Scientific Reports* **9**, 13697, <https://doi.org/10.1038/s41598-019-50116-0> (2019).
- Wang, J. Y., Liu, B. S. & Nakata, K. Effects of crystallinity, {001}/{101} ratio, and Au decoration on the photocatalytic activity of anatase TiO_2 crystals. *Chinese Journal of Catalysis* **40**, 403–412, [https://doi.org/10.1016/S1872-2067\(18\)63174-2](https://doi.org/10.1016/S1872-2067(18)63174-2) (2019).
- Di, T. M., Zhang, J. F., Cheng, B., Yu, J. G. & Xu, J. S. Hierarchically nanostructured porous TiO_2 (B) with superior photocatalytic CO_2 reduction activity. *Science China. Chemistry* **61**, 344–350, <https://doi.org/10.1007/s11426-017-9174-9> (2018).
- Szilagy, I., Konigsberger, E. & May, P. M. Characterization of chemical speciation of titanyl sulfate solutions for production of titanium dioxide precipitates. *Inorganic Chemistry* **48**, 2200–2204, <https://doi.org/10.1021/ic801722r> (2009).
- Grzmil, B., Grela, D. & Kic, B. Effects of processing parameters on hydrolysis of $TiOSO_4$. *Polish Journal of Chemical Technology* **11**, 15–21, <https://doi.org/10.2478/v10026-009-0030-1> (2009).
- Grzmil, B., Grela, D. & Kic, B. Formation of hydrated titanium dioxide from seeded titanyl sulphate solution. *Chemical Papers* **63**, 217–225, <https://doi.org/10.2478/s11696-009-0009-7> (2009).
- Tian, M. et al. Mechanism of synthesis of anatase TiO_2 pigment from low concentration of titanyl sulfuric-chloric acid solution under hydrothermal hydrolysis. *Journal of the Chinese Chemical Society* **67**, 277–287, <https://doi.org/10.1002/jccs.201900071> (2020).
- Xin, W. H. et al. A facile preparation strategy for TiO_2 spheres by direct hydrolysis. *ChemNanoMat* **5**, 1263–1266, <https://doi.org/10.1002/cnma.201900367> (2019).
- Urakaev, F. K. et al. Kinetics of homogeneous nucleation of monodispersed spherical sulfur and anatase particles in water-acid systems. *Journal of Crystal Growth* **205**, 223–232, [https://doi.org/10.1016/S0022-0248\(99\)00236-5](https://doi.org/10.1016/S0022-0248(99)00236-5) (1999).
- Zhao, G. et al. Use of ultrasound in the washing process of titania pigment production: Water saving and process optimization. *Chemical Engineering Communications* **203**, 1207–1215, <https://doi.org/10.1080/00986445.2016.1160226> (2016).
- Ohenoja, K., Illikainen, M. & Niinimäki, J. Effect of operational parameters and stress energies on the particle size distribution of TiO_2 pigment in stirred media milling. *Powder Technology* **234**, 91–96, <https://doi.org/10.1016/j.powtec.2012.09.038> (2013).
- Baneshi, M., Gonome, H., Komiya, A. & Maruyama, S. The effect of particles size distribution on aesthetic and thermal performances of polydisperse TiO_2 pigmented coatings: Comparison between numerical and experimental results. *Journal of Quantitative Spectroscopy & Radiative Transfer* **113**, 594–606, <https://doi.org/10.1016/j.jqsrt.2012.02.006> (2012).
- Zhang, W., Ou, C. R. & Yuan, Z. G. Precipitation and growth behaviour of metatitanic acid particles from titanium sulfate solution. *Powder Technology* **315**, 31–36, <https://doi.org/10.1016/j.powtec.2017.03.047> (2017).
- Jalili, M. M., Davoudi, K., Sedigh, E. Z. & Farrokhpay, S. Surface treatment of TiO_2 nanoparticles to improve dispersion in non-polar solvents. *Advanced Powder Technology* **27**, 2168–2174, <https://doi.org/10.1016/j.apt.2016.07.030> (2016).
- Tian, C. X., Huang, S. H. & Yang, Y. Anatase TiO_2 white pigment production from unenriched industrial titanyl sulfate solution via short sulfate process. *Dyes and Pigments* **96**, 609–613, <https://doi.org/10.1016/j.dyepig.2012.09.016> (2013).
- Tian, C. X. Calcination intensity on rutile white pigment production via short sulfate process. *Dyes and Pigments* **133**, 60–64, <https://doi.org/10.1016/j.dyepig.2016.05.034> (2016).
- Chen, H. L., Wang, Y. R. & Shi, J. Preparation of monodispersed superfine titanium dioxide particles and size control. *Acta. Physico-Chimica Sinica* **17**, 713–717, <https://doi.org/10.3866/PKU.WHXB20010809> (2001).

Acknowledgements

This study was funded by the National Natural Science Foundation of China (50804025), Science and Technology Project of Sichuan Province, China (2014JY0197, 2011GZ0303), Science and Technology Project of Panzhihua, China (2017CY-G-20, 2018CY-G-16, 20180816, 201810), the Opening Project of Key Laboratory of Green Chemistry of Sichuan Institutes of Higher Education (LYJ1907), Provincial and Municipal Talents Training Projects of Sichuan Province (2012).

Author contributions

Congxue Tian wrote the main manuscript text and prepared all the figures and all the tables. And Congxue Tian reviewed the manuscript.

Competing interests

The author declares no competing interests.

Additional information

Correspondence and requests for materials should be addressed to C.T.

Reprints and permissions information is available at www.nature.com/reprints.

Publisher's note Springer Nature remains neutral with regard to jurisdictional claims in published maps and institutional affiliations.



Open Access This article is licensed under a Creative Commons Attribution 4.0 International License, which permits use, sharing, adaptation, distribution and reproduction in any medium or format, as long as you give appropriate credit to the original author(s) and the source, provide a link to the Creative Commons license, and indicate if changes were made. The images or other third party material in this article are included in the article's Creative Commons license, unless indicated otherwise in a credit line to the material. If material is not included in the article's Creative Commons license and your intended use is not permitted by statutory regulation or exceeds the permitted use, you will need to obtain permission directly from the copyright holder. To view a copy of this license, visit <http://creativecommons.org/licenses/by/4.0/>.

© The Author(s) 2020